Chemical Engineering Journal 493 (2024) 152442

Contents lists available at ScienceDirect

Chemical Engineering Journal

journal homepage: www.elsevier.com/locate/cej

Efficient separation of methanol-to-olefins products using a metal-organic framework with supramolecular binding sites

Zhengyi Di [a,b], Zhenyu Ji [a], Cheng Chen [a], Rajamani Krishna [c], Daqiang Yuan [a], Maochun Hong [a], Mingyan Wu [a,d,*]

[a] State Key Lab of Structure Chemistry, Fujian Institute of Research on the Structure of Matter, CAS Institution, Fuzhou 350002, China
[b] College of Chemistry, Tianjin Key Laboratory of Structure and Performance for Functional Molecules, Tianjin Normal University Tianjin 300387, China
[c] Van 't Hoff Institute for Molecular Sciences, University of Amsterdam, Science Park 904, 1098 XH Amsterdam, the Netherlands
[d] University of Chinese Academy of Sciences, Beijing 100049, China

ARTICLE INFO

Keywords:
C_3H_6/C_2H_4 separation
Supramolecular binding sites
Cage-like
Porous materials

ABSTRACT

With the development of the methanol-to-olefins (MTO) process, research focus on the C_3H_6/C_2H_4 separation has become more urgent. The separation process based on physical adsorption has been widely studied due to its environmentally friendly and energy-efficient advantage. Herein, we reported a cage-like metal–organic framework which exhibits both high C_3H_6 adsorption capacity and excellent C_3H_6/C_2H_4 selectivity even at high temperatures. Dynamic breakthrough experiment shows it can realize the one-step acquisition of polymer-grade C_2H_4 (99.95 %) with an ultra-high productivity of 85.8 L•kg^{-1} at 298 K. Meanwhile, high purity C_3H_6 (99.5 %) can also be obtained in the desorption step, with a high productivity of 75.5 L•Kg^{-1}. More importantly, both C_2H_4 and C_3H_6 yields can still be maintained even at high temperatures or with high gas flow rates, which is rarely reported and of great value for practical applications. Furthermore, density functional theory (DFT) simulation reveals that supramolecular binding sites play the key role in the remarkable C_3H_6/C_2H_4 separation performance.

1. Introduction

As one of the most important raw materials for the chemical industry, ethylene (C_2H_4) is an essential raw material for production of organic products such as synthetic fibers, rubber and polyvinyl chloride [1–3]. In 2023, its total annual production will exceed 200 million tons and is still growing at a rate of 5 % [4–6]. Meanwhile, propylene (C_3H_6) is the second largest volume hydrocarbon in the world [7,8]. Furthermore, C_3H_6 occupies a vital position in the production of products for the chemical industry as it is a commercially important precursor for higher-value chemicals [9,10]. In the traditional industrial production, low carbon olefins are usually prepared by thermal cracking of petroleum hydrocarbons in the petroleum route, which is heavily rely on crude oil [11–14]. The dramatic fluctuations in crude oil prices and declining reserves have a huge impact on C_2H_4 and C_3H_6 production [15].

The methanol-to-olefins (MTO) process, a newly emerging and attractive technology, is an important means to realize the conversion of coal chemicals to petrochemical products [16–21]. Furthermore, using MTO process to consume methanol and produce olefin as the entry point can effectively alleviate the problem of excess methanol production [22]. In the MTO process, 51.10 wt% C_2H_4 and 20.91 wt% C_3H_6 are produced [23,24]. However, the low purity of C_2H_4 and C_3H_6 does not meet the requirement for the industrial applications. For example, the production of ethylbenzene requires high purity C_2H_4, with a volume fraction of C_3H_6 less than 0.15 % [25]. The conventional separation of C_3H_6/C_2H_4 mixtures is based on cryogenic distillation with different vapor pressures and high energy consumption [19,26]. Additionally, the traditional separation method of MTO products is alkaline washing, which generates large amounts of butter and affects equipment safety [27]. Compared with cryogenic distillation and alkaline washing techniques, adsorption-based separation is safer and more energy efficient [20,25]. The separation step can be used to obtain polymer grade C_2H_4 and the desorption step to obtain high purity C_3H_6, thus maximizing economic efficiency and improving energy efficiency. Therefore, the preparation of porous materials for highly selective adsorption of C_3H_6 is important to achieve safe and efficient separation of C_3H_6/C_2H_4.

Metal-organic frameworks (MOFs) have been widely investigated as a new kind of promising adsorbents for the separation of light

* Corresponding author at: State Key Lab of Structure Chemistry, Fujian Institute of Research on the Structure of Matter, CAS Institution, Fuzhou 350002, China.
E-mail address: wumy@fjirsm.ac.cn (M. Wu).

https://doi.org/10.1016/j.cej.2024.152442
Received 5 March 2024; Received in revised form 15 May 2024; Accepted 20 May 2024
Available online 21 May 2024

hydrocarbons mixtures, such as C_2H_2/CO_2 [28–30], C_2H_2/C_2H_4 [31,32], C_2H_4/C_2H_6 [33] and C_3H_4/C_3H_6 [34,35]. However, there are relatively few studies on the separation of C_3H_6/C_2H_4 mixtures. Actually, the separation of C_2H_4 from C_3H_6/C_2H_4 is much challenging in view of their similar sizes and physical properties [36]. Considering that C_3H_6 have more C-H groups than C_2H_4, it is necessary to establish accessible supramolecular binding sites to capture C_3H_6 and thus effectively improve the separation efficiency of C_3H_6/C_2H_4. As we know, the cage-like space is one of the important ways to improve gas adsorption and separation capacity. For example, Li et al. achieved an effective separation of C_2H_2/CO_2 by the suitable pore cages decorated with high-density supramolecular binding sites [37]. The suitable windows which can selectively capture gas molecules and cage-like spaces which can accommodate more gas molecules, work together to achieve efficient purification of C_2H_4 while having high C_3H_6 adsorption capacity. Thus, high C_2H_4 separation performance and high C_3H_6 desorption capacity can be achieved in one separation cycle.

With the above thought in mind, herein we report a metal − organic framework (FJI-H8-Me) which exhibits high C_3H_6 adsorption capacity especially at low pressure. Dynamic breakthrough experiments demonstrate that it exhibits excellent C_3H_6/C_2H_4 separation performance and can realize the one-step acquisition of polymer-grade C_2H_4 with an ultra-high productivity of 85.8 L•kg^{-1} at 298 K. In the meantime, high purity C_3H_6 (99.5 %) can also be obtained in the desorption step with a high productivity of 75.5 L•kg^{-1}. Surprisingly, raising the temperature from 298 K to 338 K or increasing the flow rates of the gas mixture barely affects the yields of C_2H_4 and C_3H_6. Furthermore, density functional theory (DFT) simulation reveals that the windows of the cages have much more supramolecular interactions with C_3H_6 than C_2H_4, which play the key role in the remarkable C_3H_6/C_2H_4 separation performance. We think this supramolecular binding sites strategy provides a new way to design porous materials with excellent C_3H_6/C_2H_4 separation performance.

2. Experimental methods

2.1. Gas sorption experiment

All gas sorption isotherms were measured with a Micromeritics ASAP 2020-M surface area and pore size analyser. The fresh crystalline sample of FJI-H8-Me was followed solvent exchange with methanol and then dichloromethane for 3 days and evacuation of the dichloromethane by heating at 80 °C for 10 h under a high vacuum. The nitrogen sorption isotherm was collected at 77 K in a liquid nitrogen bath. The specific surface areas were determined using the Brunauer–Emmett–Teller model from the N_2 sorption data. For selective adsorption evaluation, the gas sorption experiments of C_2H_4 and C_3H_6 were carried out at 273 K in an ice − water bath, and at 298 K, 303 K, 308 K, 318 K, 328 K, 338 K in a liquid bath, respectively. The isosteric heat of adsorption was calculated through the Clausius–Clapeyron equation using the four sets of acetylene adsorption data collected.

2.2. Breakthrough measurements

Breakthrough experiments for the separation of C_3H_6/C_2H_4 (v/v, 50/50) were carried out in a fixed bed. A stainless-steel column with a length of 180 mm and an internal diameter of 3 mm was used for sample packing. The flow rates of all gases are regulated by mass flow controllers, and the effluent gas stream from the column is monitored by gas chromatography (GC) detector. All measurements were performed following a protocol established by literatures. The initial activated FJI-H8-Me crystals were packed into a stainless-steel column tightly. Then, the column was activated with He flow under 80 °C for 10 h. Then, a mixture flow was dosed into the column. Breakpoints were determined when the first peak was detected. For the cycling of breakthrough experiments, the sample was regenerated by desorption under He flow for 30 min at 353 K. Recovery of high purity C_3H_6 is realized during the desorption step. Experimental dynamic desorption curves of FJI-H8-Me are obtained after breakthrough experiments of C_3H_6/C_2H_4 (v/v, 50/50) with He flow rate of 15 mL/min at 80 °C.

3. Results and discussion

FJI-H8-Me has three types of polyhedral nanocage, i.e., regular cuboctahedron (Cage-A), distorted octahedron (Cage-B) and distorted cuboctahedron (Cage-C) (Fig. 1). One Cage-A is interconnected with eight Cage-B through eight triangular faces and as well as with six Cage-C through six rhombic faces. Furthermore, Cage-B is interconnected with four Cage-A through four triangular faces and with four Cage-C by sharing four *m*-benzenedicarboxylate moieties. Cage-C is interconnected with six Cage-A through six rhombic faces of and with eight Cage-B by sharing eight *m*-benzenedicarboxylate acid groups. Finally, the above different molecular cages are stacked to form a three-dimensional porous framework structure. If we consider Cage-A, Cage-B and Cage-C as a 14-connected node, an 8-connected node and a 14-connected node respectively, FJI-H8-Me has a rarely seen (8,14,14)-connected framework.

The permanent porosity of activated FJI-H8-Me was established by nitrogen (N_2) adsorption isotherms at 77 K, which revealed that FJI-H8-Me exhibits a typically reversible type-I behavior (Figure S4), the Brunauer– Emmett–Teller surface area is 2054 ± 6 m^2/g. Motivated by the cage-like structure of FJI-H8-Me, the single component adsorption isotherms at 273, 298, 303, 308, 318, 328 and 338 K were tested to evaluate its C_3H_6/C_2H_4 separation performance. As shown in Fig. 2a and 2b, compared with C_2H_4 the adsorption isotherms of C_3H_6 show a distinct sharp step at relatively low pressures in the range of 273 K − 338 K. For example, the C_3H_6 uptake is 100.7 cm^3 g^{-1} and the C_2H_4 uptake is 15.9 cm^3 g^{-1}at 298 K under 2 kPa, with the C_3H_6/C_2H_4 uptake ratio of 6.3. In particular, the adsorption capacity of C_3H_6 reached 156.1 cm^3 g^{-1} at 298 K under 10 kPa, surpassing most reported outstanding materials, such as Zn-BPZ-SA (46.6 cm^3 g^{-1}) [38], *iso*-MOF-4 (57.9 cm^3 g^{-1}) [25], $Zn_2(oba)_2(dmimpym)$ (56.0 cm^3 g^{-1}) [39], spe-MOF (41.5 cm^3 g^{-1}) [40], NKMOF-11 (33 cm^3 g^{-1}) [41], and Mn-dtzip (86.3 cm^3 g^{-1}) [42]. In comparison, the C_2H_4 uptake increases slowly with the increase of pressure and shows lower adsorption capacity of 55.1 cm^3 g^{-1} under the same condition. Such big difference between C_3H_6 and C_2H_4 uptakes manifests that FJI-H8-Me has great potential to efficiently separate C_3H_6/C_2H_4 mixtures. In addition, when the test temperature is raised to 338 K, the single component adsorption isotherm for C_3H_6 does not have major change compared with that at 298 K. The uptake of C_3H_6 is still up to 181.3 cm^3 g^{-1} at 338 K and 100 kPa (211.0 cm^3 g^{-1} at 298 K). In comparison, the single component adsorption isotherm for C_2H_4 has obvious decrease. The adsorption capacity of C_2H_4 decreases to 121.1 cm^3 g^{-1} at 338 K and 100 kPa (173.1 cm^3 g^{-1} at 298 K). The above results indicated that FJI-H8-Me may have good C_3H_6/C_2H_4 separation performance even at high temperatures.

It is well-known that the magnitude of the adsorption heats of porous materials reveals the affinity of the pore surface toward the adsorbates. To evaluate the affinity of C_3H_6 and C_2H_4 to FJI-H8-Me, the adsorption heats (Q_{st}) were calculated by the Clausius − Clapeyron equation. As shown in the Fig. 2c, the Q_{st} for C_3H_6 is in the range of 44.3——26.3 kJ mol^{-1}, which is obviously higher than those for C_2H_4 (34.3 – 25.2 kJ mol^{-1}). The stronger affinity of FJI-H8-Me for C_3H_6 will lead to the preferential capture for C_3H_6 over C_2H_4 in the separation process. Meanwhile, the Q_{st} value of C_3H_6 is moderately high and lower than most MOFs such as srl-MOF (44.7——35.9 kJ mol^{-1}) [40], ANPC-2–700 (54.2——33.1 kJ mol^{-1}) [43], SIFSIX-3-Ni (54.7—47.1 kJ mol^{-1}) [44] and JNU-3a (44.6——36.2 kJ mol^{-1}) [9]. Such moderate Q_{st} endows the preferential C_3H_6 adsorption as well as facile recovery of C_3H_6 under mild conditions with a low energy input during the desorption process. Therefore, the separation and desorption steps yield high purity C_2H_4 and C_3H_6 respectively, minimizing energy waste and improving the

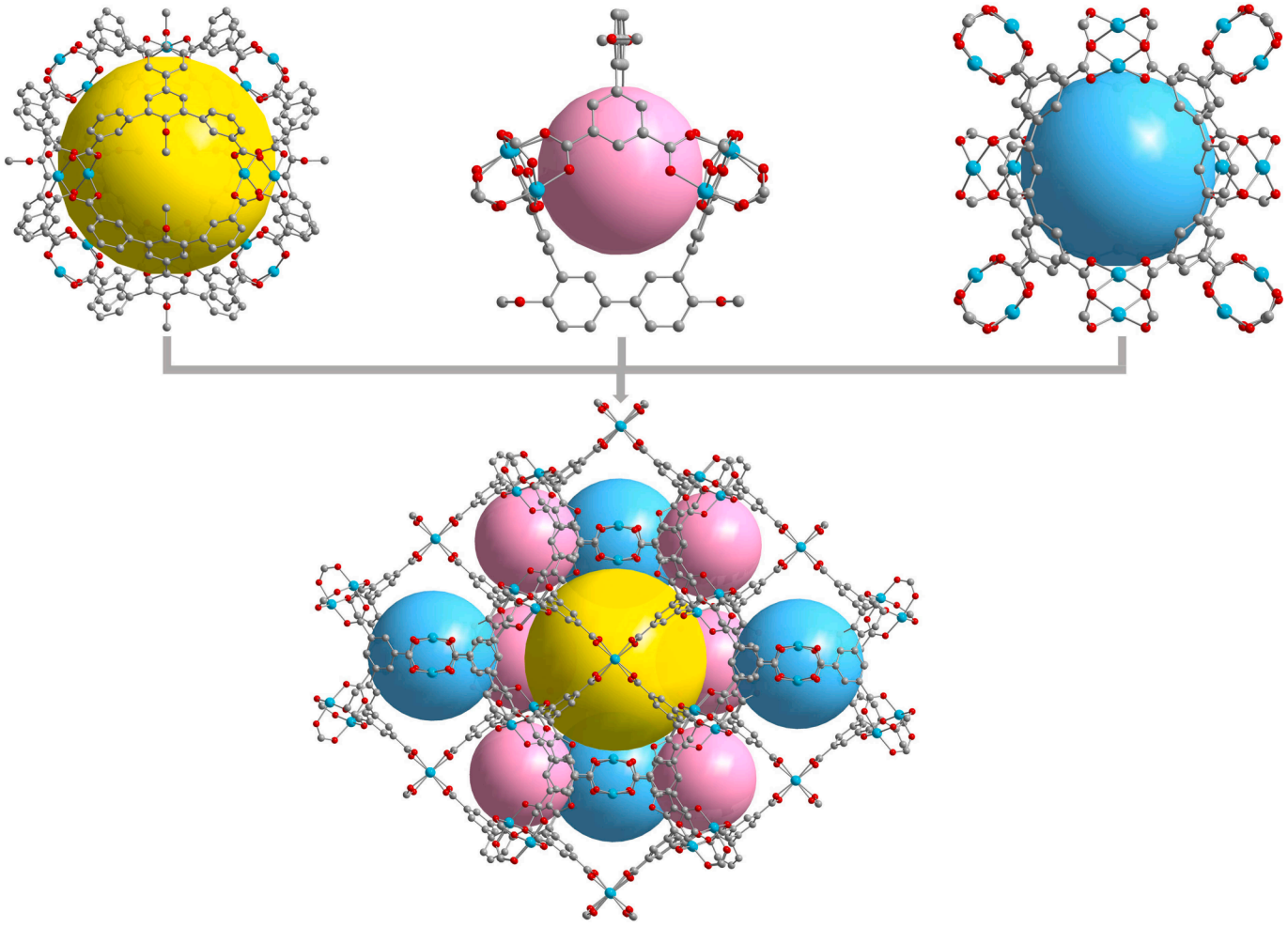

Fig. 1. Structure description of FJI-H8-Me. View of three types of polyhedral nanocages and the combination. (Yellow ball represents regular cuboctahedral Cage-A; Pink ball represents distorted octahedral Cage-B; Blue ball represents distorted cuboctahedral Cage-C). (For interpretation of the references to colour in this figure legend, the reader is referred to the web version of this article.)

efficiency of energy utilization.

To evaluate the C_3H_6/C_2H_4 separation performance of FJI-H8-Me, the ideal adsorbed solution theory (IAST) was applied to calculate the C_3H_6/C_2H_4 selectivity for the mixture of C_3H_6/C_2H_4 (50/50, v/v) at different temperatures (Fig. 2d). The result indicates that FJI-H8-Me has an exceptionally high C_3H_6/C_2H_4 selectivity (24.1 – 9.9) at 298 K, which is higher than the benchmark porous MOF materials for C_3H_6/C_2H_4 separation, such as Zn-BPZ-TATB (11.3 – 7.4) [45], Zn-BPZ-SA (7.5 – 4.8) [38], $Cu_3(OH)_2(Me_2BPZ)_2$ (2.0 – 7.4) [46], spe-MOF (9.2 – 7.7) [40], MAC-4 (10.8 – 8.4) [47] and UPC-33 (13.1 – 10.2) [48]. More importantly, there is no significant decrease in the C_3H_6/C_2H_4 selectivity when increasing the temperature. Even at 338 K, the selectivity remains 16.8——7.6. The above result also indicates that FJI-H8-Me has great potential for C_3H_6/C_2H_4 separation.

To validate the feasibility of using FJI-H8-Me to separate MTO products in a packed column, transient breakthrough simulations for C_3H_6/C_2H_4 (50/50, v/v) mixtures were done at 298 K using the methodology described by Krishna (see Supporting Information) [49–51]. The simulated curves in Fig. 3a show that the mixtures can be completely separated, whereby C_2H_4 breakthrough occurs first to yield the pure C_2H_4 but C_3H_6 passes through the column after a longer time. To evaluate the actual C_3H_6/C_2H_4 separation performance of FJI-H8-Me, we have performed the fixed-bed breakthrough tests under different conditions. During these experiments, the mixture of C_3H_6/C_2H_4 (50/50, v/v) was passed through a fixed-bed (180 mm × 3 mm) column packed with activated FJI-H8-Me. As shown in Fig. 3a, C_2H_4 passes through the packed column at 97.7 min and reaches the equilibrium with undetectable C_3H_6 (detection limit: 100 ppm) at 298 K and with a total flow rate of 2 mL min^{-1}. However, C_3H_6 does not elute until 183.5 min and then rapidly achieves the concentration of feed gas. The separation time for C_2H_4 is ca. 85.8 min. There is an excellent match between the experimental and simulated curves. Therefore, the one-step acquisition polymer-grade of C_2H_4 can be realized with a ultra-high productivity of 85.8 L kg^{-1} at 298 K, which is much higher than the benchmark C_3H_6/C_2H_4 separation materials such as Zn-BPZSA (21.9 L kg^{-1}) [38] and spe-MOF (67 L kg^{-1}) [40]. In view of the importance of the recyclability of porous materials in practical applications, cycle tests also have been carried out. As shown in Fig. 3b, FJI-H8-Me shows excellent reusability. After five-cycle C_3H_6/C_2H_4 separation experiments, FJI-H8-Me still maintains an excellent separation performance with the separation performance almost unchanged, which indicates that FJI-H8-Me has excellent stability for C_3H_6/C_2H_4 separation.

As we know, the gas flow rates usually have the influence on the gas separation performance. Therefore, the breakthrough experiments with different gas flow rates have also been investigated. As shown in Fig. 3c, at 298 K FJI-H8-Me shows an excellent separation performance when the flow rates of the mixed gas have been increased from 2.0 mL min^{-1} to 4.0 mL min^{-1} and even up to 6.0 mL min^{-1}. Accordingly, the separation times are 44.5 and 30.7 min respectively and the C_2H_4 productivities have no obvious change (Figure S5). More important, FJI-H8-Me also exhibits very good recycling performance at different flow rates (Figure S6 and S7).

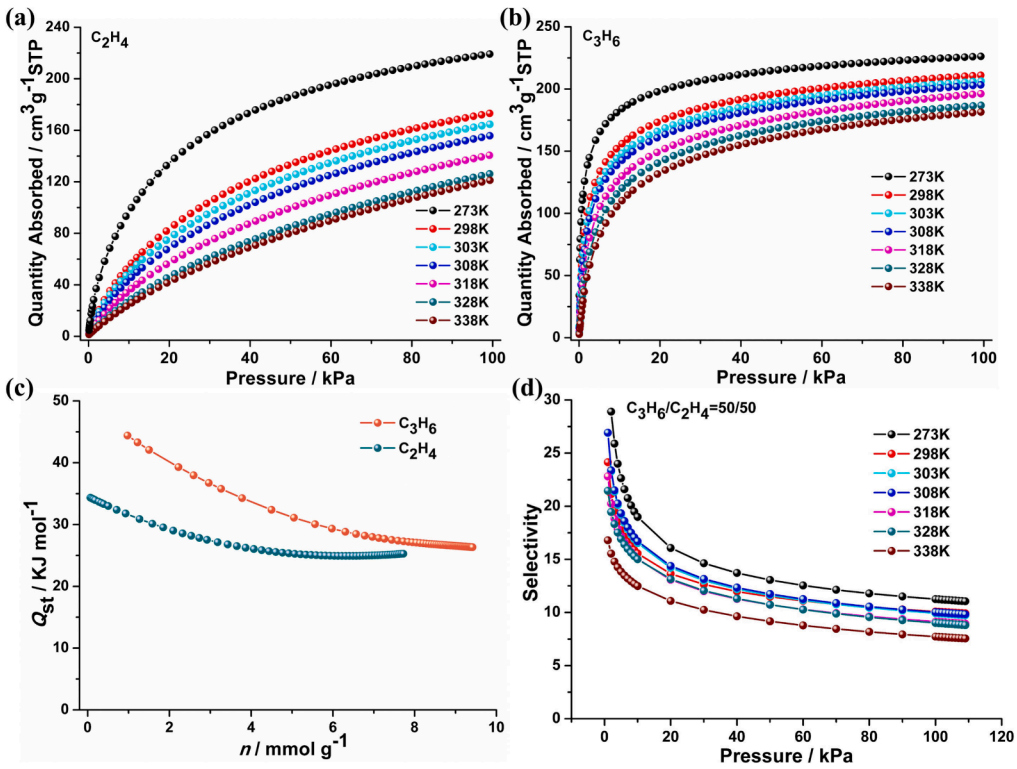

Fig. 2. (a) and (b) The C_2H_4 and C_3H_6 sorption isotherms at 273 K, 298 K, 303 K, 308 K, 318 K, 328 K and 338 K respectively; (c) Adsorption heats of FJI-H8-Me for C_2H_4 and C_3H_6 respectively; (d) The IAST selectivity of FJI-H8-Me for 50/50 C_3H_6/C_2H_4 at 273 K, 298 K, 303 K, 308 K, 318 K, 328 K and 338 K respectively.

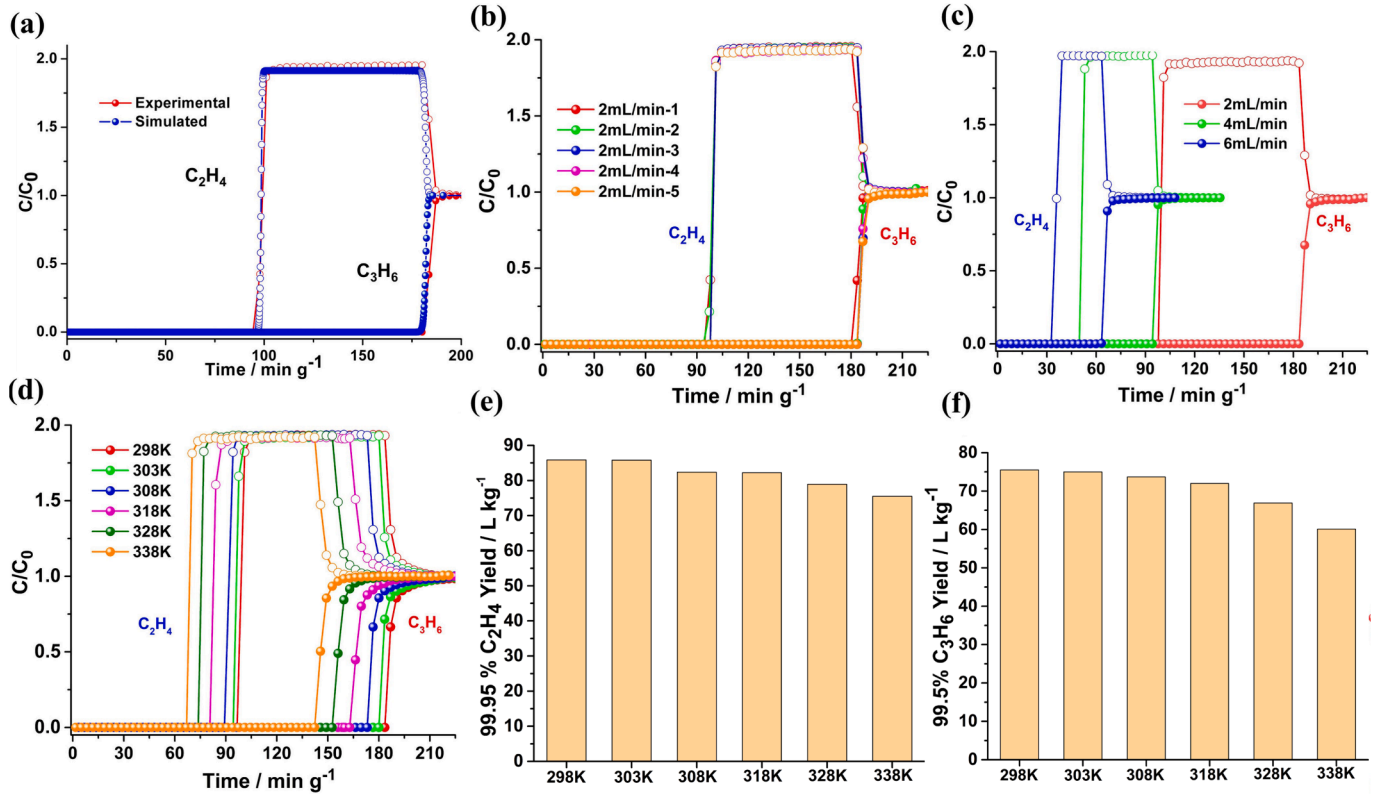

Fig. 3. Breakthrough curves of FJI-H8-Me for C_3H_6/C_2H_4 (50/50, v/v). (a) The actual and simulated breakthrough curves of FJI-H8-Me for C_3H_6/C_2H_4 separation at 298 K. (b) Five-cycle tests at 298 K with the gas flow rate of 2 mL·min^{-1}; (c) The breakthrough curves with different flow rates (2.0 mL min^{-1}, 4.0 mL min^{-1} and 6.0 mL min^{-1}) at 298 K; (d) The breakthrough curves with flow rate of 2 mL min^{-1} at different temperatures (298 K, 303 K, 308 K, 318 K, 328 K and 338 K); (e) The yields of C_2H_4 (purity ≥ 99.95 %) at different temperatures with flow rate of 2 mL min^{-1}; (f) The yields of C_3H_6 (purity ≥ 99.5 %) at different temperatures with flow rate of 2 mL min^{-1} during the desorption process.

To meet the requirement for practical application, porous materials should be able to maintain its good separation performance in a wide temperature range, even at high temperature. It is found that FJI-H8-Me can achieve excellent C_3H_6/C_2H_4 separation performance in the temperature range from 298 K to 338 K (Fig. 3d and 3e). When the temperature is raised to 318 K, the C_3H_6/C_2H_4 separation performance has no obvious change. Even at 338 K, the separation time is till up to 75.5 min. The C_2H_4 productivity is as high as 75.5 L kg^{-1}, which is much higher than the benchmark C_3H_6/C_2H_4 separation materials at 298 K (Fig. 3e). More importantly, FJI-H8-Me still has good cycle performance (Figure S8 - S12) at such high temperatures, which is rarely seen in the porous materials. This excellent C_3H_6/C_2H_4 separation performance is well consistent with the obvious difference in the single-component gas adsorption curves for C_3H_6 and C_2H_4 as well as the high IAST C_3H_6/C_2H_4 selectivity at high temperature.

A particular feature of FJI-H8-Me is that high purity C_3H_6 can be obtained during the desorption step (Fig. 3f). For example, a high C_3H_6 productivity of 75.5 L•kg^{-1} with the purity $\geq$ 99.5 % can be obtained at 298 K and with a flow rate of 2 mL min^{-1}. When raising the temperature up to 318 K, the C_3H_6 productivity does not has obvious decrease. Even at 338 K, the C_3H_6 productivity still reaches up to 60.1 L•kg^{-1}. Additionally, gas flow rates also have no obvious influence on the C_3H_6 productivities (Figure S13). Increasing the gas flow rate up to 6 mL min^{-1}, the C_3H_6 productivity can still be maintained. As we have established, the productivities of both C_2H_4 and C_3H_6 are superior to those benchmark materials for MTO product separation (Table S3). Additionally, when the feeding gas is changed to 2/5 or 1/9 (v/v) C_3H_6/C_2H_4, at 298 K FJI-H8-Me maintains good separation performance with the flow rate of 2 mL min^{-1} respectively (Figure S39). Moreover, an ideal adsorbent for practical applications should have an energy-efficient regeneration process. The repeated breakthrough experiments of FJI-H8-Me for C_3H_6/C_2H_4 were tested at room temperature with the simple activation treatment at 80 °C for 30 min (Table S3). This is comparable to the benchmark materials reported. To sum up, owing to the advantages of the simultaneous acquisition of high-purity C_2H_4 and C_3H_6 in one separation cycle, promising separation performance even at high temperatures or high flow rates, and good reusability, FJI-H8-Me has the best performance for C_3H_6/C_2H_4 separation in the porous materials so far.

In order to understand the excellent separation effect of FJI-H8-Me on C_3H_6/C_2H_4 mixture and to investigate the mechanism of gas adsorption and separation in depth, we have performed theoretical calculations to determine the adsorption sites of C_2H_4 and C_3H_6 and the details can be found in the supporting information. As shown in Fig. 4a, the strongest binding site for C_2H_4 is beside the triangular window, where the C_2H_4 molecule interacts with two phenyl rings and four carboxylic oxygen atoms through two C-H···π (2.86 and 3.25 Å) and four C-H···O (2.85, 2.91, 3.17 and 3.29 Å) interactions. As for C_3H_6 molecule, the situation is similar. The C_3H_6 interacts with three phenyl rings and six carboxylic oxygen atoms through three C-H···π (2.71, 3.00 and 3.81 Å) and six C-H···O (2.95, 3.17, 3.29, 3.47, 3.48 and 3.49 Å) interactions (Fig. 4b). Though both C_2H_4 and C_3H_6 primarily interact with the supramolecular binding sites, it is obvious that there are significantly stronger interactions between C_3H_6 molecule and the framework. Furthermore, the calculated static binding energy for C_3H_6 is 87.45 kJ mol^{-1}, which is higher than that for C_2H_4 (63.34 kJ mol^{-1}). The obvious difference between the static binding energies for C_3H_6 and C_2H_4 makes the supramolecular binding site preferentially capture C_3H_6 rather than C_2H_4 and promises the excellent performance for C_3H_6/C_2H_4 separation.

4. Conclusion

In summary, we have reported a porous cage-like material which has much higher C_3H_6 uptake than C_2H_4 especially at low pressure. Dynamic breakthrough studies show that it exhibits excellent C_3H_6/C_2H_4 separation performance. A particular feature of FJI-H8-Me is that polymer-grade C_2H_4 and C_3H_6 can be obtained with ultra-high productivities in one separation cycle. It can realize one-step acquisition of polymer-grade C_2H_4 ($\geq$99.95 %) with a productivity of 85.8 L•kg^{-1}. Meanwhile, high purity C_3H_6 ($\geq$99.5 %) with a productivity of 75.5 L•kg^{-1} can be obtained during the desorption step. Surprisingly, both temperature and flow rate have almost no effect on the yield of C_2H_4 and C_3H_6, which is rarely seen. Furthermore, theoretical calculation reveals that the supramolecular binding site adjacent to the triangular window can preferentially capture C_3H_6 and contributes much to the excellent separation performance. Therefore, FJI-H8-Me is considered as a promising material which can be used for energy-efficient separation of MTO products. In summary, we believe this supramolecular binding site strategy provides a new way to design high-performance MOF materials with excellent C_3H_6/C_2H_4 separation performance in the future.

CRediT authorship contribution statement

Zhengyi Di: Writing – original draft, Project administration, Funding acquisition, Formal analysis, Data curation. **Zhenyu Ji:** Formal analysis. **Cheng Chen:** Methodology. **Rajamani Krishna:** Methodology.

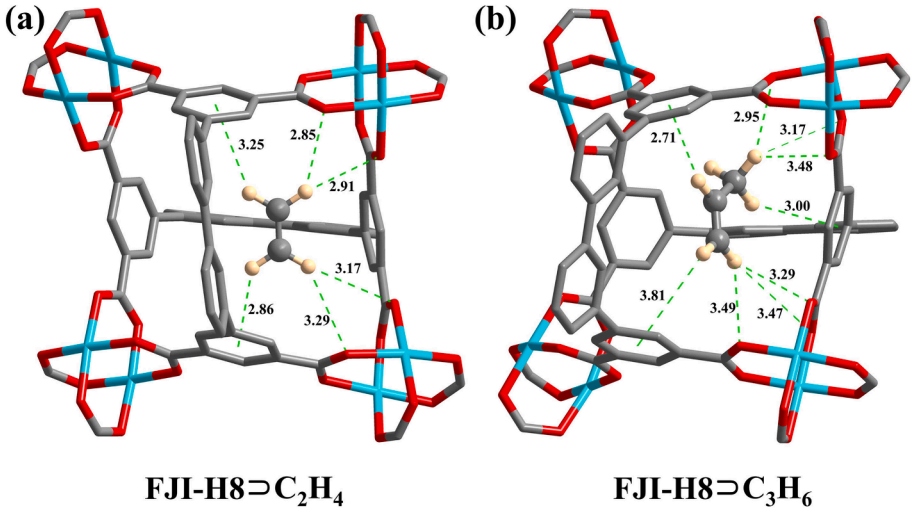

Fig. 4. The calculated optimized adsorption sites for C_2H_4 (a) and C_3H_6 (b) in FJI-H8-Me. (C, gray; O, red; Cu, blue; H, tan. The weak interactions are shown in green dashed lines). For clarity, the H atoms in benzene rings are omitted. (For interpretation of the references to colour in this figure legend, the reader is referred to the web version of this article.)

Daqiang Yuan: Software. **Maochun Hong:** Supervision. **Mingyan Wu:** Writing – review & editing, Supervision, Funding acquisition, Conceptualization.

Declaration of competing interest

The authors declare that they have no known competing financial interests or personal relationships that could have appeared to influence the work reported in this paper.

Data availability

Data will be made available on request.

Acknowledgements

We acknowledge the financial supports of the National Nature Science Foundation of China (22205163). Additionally, this work is also supported by the Self-deployment Project Research Program of Haixi Institutes, Chinese Academy of Sciences with the grant number of CXZX-2022-JQ04.

Appendix A. Supplementary data

Supplementary data to this article can be found online at https://doi.org/10.1016/j.cej.2024.152442.

References

[1] L. Li, R.B. Lin, R. Krishna, H. Li, S. Xiang, H. Wu, J. Li, W. Zhou, B. Chen, Ethane/ethylene separation in a metal-organic framework with iron-peroxo sites, Science 362 (2018) 443–446, https://doi.org/10.1126/science.aat0586.

[2] L. Wang, H. Huang, X. Zhang, H. Zhao, F. Li, Y. Gu, Designed metal-organic frameworks with potential for multi-component hydrocarbon separation, Coord. Chem. Rev. 484 (2023) 215111, https://doi.org/10.1016/j.ccr.2023.215111.

[3] Y.-Y. Xiong, C.-X. Chen, T. Pham, Z.-W. Wei, K.A. Forrest, M. Pan, C.-Y. Su, Dynamic Spacer Installation of Multifunctionalities into Metal–Organic Frameworks for Spontaneous One-Step Ethylene Purification from a Ternary C_2-Hydrocarbons Mixture, CCS Chem. 6 (2023) 241–254. 10.31635/ccschem.023.202302698.

[4] A. Ebadi Amooghin, H. Sanaeepur, R. Luque, H. Garcia, B. Chen, Fluorinated metal-organic frameworks for gas separation, Chem. Soc. Rev. 51 (2022) 7427–7508, https://doi.org/10.1039/d2cs00442a.

[5] Z. Di, C. Liu, J. Pang, S. Zou, Z. Ji, F. Hu, C. Chen, D. Yuan, M. Hong, M. Wu, A Metal-Organic Framework with Nonpolar Pore Surfaces for the One-step Acquisition of C_2H_4 from a C_2H_4 and C_2H_6 Mixture, Angew. Chem. Int. Ed. 61 (2022) e202210343.

[6] W. Liang, Z. Luo, Z. Liu, X. Wei, W. Cai, Nitrogen-doped carbon particles with distinctive ethylene adsorption selectivity for efficient ethylene/acetylene separation, Chem. Eng. J. 477 (2023) 147220, https://doi.org/10.1016/j.cej.2023.147220.

[7] D. Liu, J. Pei, X. Zhang, X.W. Gu, H.M. Wen, B. Chen, G. Qian, B. Li, Scalable Green Synthesis of Robust Ultra-Microporous Hofmann Clathrate Material with Record C_3H_6 Storage Density for Efficient C_3H_6/C_3H_8 Separation, Angew. Chem. Int. Ed. 62 (2023) e202218590.

[8] Q. Dong, Y. Huang, J. Wan, Z. Lu, Z. Wang, C. Gu, J. Duan, J. Bai, Confining Water Nanotubes in a $Cu_{10}O_{13}$-Based Metal-Organic Framework for Propylene/Propane Separation with Record-High Selectivity, J. Am. Chem. Soc. 145 (2023) 8043–8051, https://doi.org/10.1021/jacs.3c00515.

[9] H. Zeng, M. Xie, T. Wang, R.-J. Wei, X.-J. Xie, Y. Zhao, W. Lu, D. Li, Orthogonal-array dynamic molecular sieving of propylene/propane mixtures, Nature 595 (2021) 542–548, https://doi.org/10.1038/s41586-021-03627-8.

[10] Y.L. Peng, C. He, T. Pham, T. Wang, P. Li, R. Krishna, K.A. Forrest, A. Hogan, S. Suepaul, B. Space, M. Fang, Y. Chen, M.J. Zaworotko, J. Li, L. Li, Z. Zhang, P. Cheng, B. Chen, Robust Microporous Metal-Organic Frameworks for Highly Efficient and Simultaneous Removal of Propyne and Propadiene from Propylene, Angew. Chem. Int. Ed. 58 (2019) 10209–10214, https://doi.org/10.1002/anie.201904312.

[11] F. Jiao, J. Li, X. Pan, J. Xiao, H. Li, H. Ma, M. Wei, Y. Pan, Z. Zhou, M. Li, S. Miao, J. Li, Y. Zhu, D. Xiao, T. He, J. Yang, F. Qi, Q. Fu, X. Bao, Selective conversion of syngas to light olefins, Science 351 (2016) 1065–1068, https://doi.org/10.1126/science.aaf1835.

[12] Y. Ye, Y. Xie, Y. Shi, L. Gong, J. Phipps, A.M. Al-Enizi, A. Nafady, B. Chen, S. Ma, A Microporous Metal-Organic Framework with Unique Aromatic Pore Surfaces for High Performance C_2H_6/C_2H_4 Separation, Angew. Chem. Int. Ed. 62 (2023) e202302564.

[13] O.T. Qazvini, R. Babarao, Z.L. Shi, Y.B. Zhang, S.G. Telfer, A Robust Ethane-Trapping Metal-Organic Framework with a High Capacity for Ethylene Purification, J. Am. Chem. Soc. 141 (2019) 5014–5020, https://doi.org/10.1021/jacs.9b00913.

[14] L. Feng, Y.-X. Tan, E.-S.M. El-Sayed, F. Qiu, W. Wang, K. Su, D. Yuan, Robust Giant Octahedral [6+8] Porous Organic Cages for Efficient Ethylene/Ethane Separation, CCS Chem. (2024). 10.31635/ccschem.024.202303625.

[15] I. Yarulina, K. De Wispelaere, S. Bailleul, J. Goetze, M. Radersma, E. Abou-Hamad, I. Vollmer, M. Goesten, B. Mezari, E.J.M. Hensen, J.S. Martinez-Espin, M. Morten, S. Mitchell, J. Perez-Ramirez, U. Olsbye, B.M. Weckhuysen, V. Van Speybroeck, F. Kapteijn, J. Gascon, Structure-performance descriptors and the role of Lewis acidity in the methanol-to-propylene process, Nat. Chem. 10 (2018) 804–812, https://doi.org/10.1038/s41557-018-0081-0.

[16] X. Wu, Z. Zhang, Z. Pan, X. Zhou, A. Bodi, P. Hemberger, Ketenes in the Induction of the Methanol-to-Olefins Process, Angew. Chem. Int. Ed. 61 (2022) e202207777.

[17] M.R. Gogate, Methanol-to-olefins process technology: current status and future prospects, Petrol, Sci. Technol. 37 (2019) 559–565, https://doi.org/10.1080/10916466.2018.1555589.

[18] C. Wang, Y. Chu, M. Hu, W. Cai, Q. Wang, G. Qi, S. Li, J. Xu, F. Deng, Insight into Carbocation-Induced Noncovalent Interactions in the Methanol-to-Olefins Reaction over ZSM-5 Zeolite by Solid-State NMR Spectroscopy, Angew. Chem. Int. Ed. 60 (2021) 26847–26854, https://doi.org/10.1002/anie.202112948.

[19] A. Cesarini, S. Mitchell, G. Zichittella, M. Agrachev, S.P. Schmid, G. Jeschke, Z. Pan, A. Bodi, P. Hemberger, J. Perez-Ramirez, Elucidation of radical- and oxygenate-driven paths in zeolite-catalysed conversion of methanol and methyl chloride to hydrocarbons, Nat. Catal. 5 (2022) 605–614, https://doi.org/10.1038/s41929-022-00808-0.

[20] P. Schwach, X. Pan, X. Bao, Direct Conversion of Methane to Value-Added Chemicals over Heterogeneous Catalysts: Challenges and Prospects, Chem. Rev. 117 (2017) 8497–8520, https://doi.org/10.1021/acs.chemrev.6b00715.

[21] U. Olsbye, S. Svelle, M. Bjorgen, P. Beato, T.V. Janssens, F. Joensen, S. Bordiga, K. P. Lillerud, Conversion of methanol to hydrocarbons: how zeolite cavity and pore size controls product selectivity, Angew. Chem. Int. Ed. 51 (2012) 5810–5831, https://doi.org/10.1002/anie.201103657.

[22] C. Wang, L. Yang, M. Gao, X. Shao, W. Dai, G. Wu, N. Guan, Z. Xu, M. Ye, L. Li, Directional Construction of Active Naphthalenic Species within SAPO-34 Crystals toward More Efficient Methanol-to-Olefin Conversion, J. Am. Chem. Soc. 144 (2022) 21408–21416, https://doi.org/10.1021/jacs.2c10495.

[23] X.H. Han, K. Gong, X. Huang, J.W. Yang, X. Feng, J. Xie, B. Wang, Syntheses of Covalent Organic Frameworks via a One-Pot Suzuki Coupling and Schiff's Base Reaction for C_2H_4/C_3H_6 Separation, Angew. Chem. Int. Ed. 134 (2022) e202202912.

[24] S. Peng, M. Gao, H. Li, M. Yang, M. Ye, Z. Liu, Control of Surface Barriers in Mass Transfer to Modulate Methanol-to-Olefins Reaction over SAPO-34 Zeolites, Angew. Chem. Int. Ed. 59 (2020) 21945–21948, https://doi.org/10.1002/anie.202009230.

[25] W. Fan, X. Wang, X. Zhang, X. Liu, Y. Wang, Z. Kang, F. Dai, B. Xu, R. Wang, D. Sun, Fine-Tuning the Pore Environment of the Microporous Cu-MOF for High Propylene Storage and Efficient Separation of Light Hydrocarbons, ACS Cent. Sci. 5 (2019) 1261–1268, https://doi.org/10.1021/acscentsci.9b00423.

[26] P. Tian, Y. Wei, M. Ye, Z. Liu, Methanol to Olefins (MTO): From Fundamentals to Commercialization, ACS Catal. 5 (2015) 1922–1938, https://doi.org/10.1021/acscatal.5b00007.

[27] X. Liu, C. Hao, J. Li, Y. Wang, Y. Hou, X. Li, L. Zhao, H. Zhu, W. Guo, An anionic metal–organic framework: metathesis of Zinc(II) with Copper(II) for efficient C_3/C_2 hydrocarbon and organic dye separation, Inorg. Chem. Front. 5 (2018) 2898–2905, https://doi.org/10.1039/c8qi00773j.

[28] Z. Di, C. Liu, J. Pang, C. Chen, F. Hu, D. Yuan, M. Wu, M. Hong, Cage-like Porous Materials with Simultaneous High C_2H_2 Storage and Excellent C_2H_2/CO_2 Separation Performance, Angew. Chem. Int. Ed. 60 (2021) 10828–10832, https://doi.org/10.1002/anie.202101907.

[29] Y. Ye, S. Xian, H. Cui, K. Tan, L. Gong, B. Liang, T. Pham, H. Pandey, R. Krishna, P. C. Lan, K.A. Forrest, B. Space, T. Thonhauser, J. Li, S. Ma, Metal-Organic Framework Based Hydrogen-Bonding Nanotrap for Efficient Acetylene Storage and Separation, J. Am. Chem. Soc. 144 (2022) 1681–1689, https://doi.org/10.1021/jacs.1c10620.

[30] T. Ke, Q. Wang, X. Zhu, J. Hu, Z. Bao, Z. Zhang, Q. Ren, Q. Yang, High-capacity dynamic exclusion for highly efficient dilute C_2H_2 separation from CO_2 and multicomponent mixture in robust ultramicroporous MOF by topology regulation, Chem. Eng. J. 472 (2023) 144852, https://doi.org/10.1016/j.cej.2023.144852.

[31] J. Pei, K. Shao, J.X. Wang, H.M. Wen, Y. Yang, Y. Cui, R. Krishna, B. Li, G. Qian, A Chemically Stable Hofmann-Type Metal-Organic Framework with Sandwich-Like Binding Sites for Benchmark Acetylene Capture, Adv. Mater. 32 (2020) 1908275, https://doi.org/10.1002/adma.201908275.

[32] Z. Zhang, S.B. Peh, Y. Wang, C. Kang, W. Fan, D. Zhao, Efficient Trapping of Trace Acetylene from Ethylene in an Ultramicroporous Metal-Organic Framework via Synergistic Effect of High-Density Open Metal Sites and Electronegative Sites, Angew. Chem. Int. Ed. 59 (2020) 18927–18932, https://doi.org/10.1002/anie.202009446.

[33] W. Liu, S. Geng, N. Li, S. Wang, S. Jia, F. Jin, T. Wang, K.A. Forrest, T. Pham, P. Cheng, Y. Chen, J.G. Ma, Z. Zhang, Highly Robust Microporous Metal-Organic Frameworks for Efficient Ethylene Purification under Dry and Humid Conditions, Angew. Chem. Int. Ed. 62 (2023) e202217662.

[34] M.Y. Gao, A.A. Bezrukov, B.Q. Song, M. He, S.J. Nikkhah, S.Q. Wang, N. Kumar, S. Darwish, D. Sensharma, C. Deng, J. Li, L. Liu, R. Krishna, M. Vandichel, S. Yang, M.J. Zaworotko, Highly Productive C_3H_4/C_3H_6 Trace Separation by a Packing

Polymorph of a Layered Hybrid Ultramicroporous Material, J. Am. Chem. Soc. 145 (2023) 11837–11845, https://doi.org/10.1021/jacs.3c03505.
[35] L. Li, H.M. Wen, C. He, R.B. Lin, R. Krishna, H. Wu, W. Zhou, J. Li, B. Li, B. Chen, A Metal-Organic Framework with Suitable Pore Size and Specific Functional Sites for the Removal of Trace Propyne from Propylene, Angew. Chem. Int. Ed. 57 (2018) 15183–15188, https://doi.org/10.1002/anie.201809869.
[36] S. Gao, C.G. Morris, Z. Lu, Y. Yan, H.G.W. Godfrey, C. Murray, C.C. Tang, K. M. Thomas, S. Yang, M. Schröder, Selective Hysteretic Sorption of Light Hydrocarbons in a Flexible Metal-Organic Framework Material, Chem. Mater. 28 (2016) 2331–2340, https://doi.org/10.1021/acs.chemmater.6b00443.
[37] K. Shao, H.-M. Wen, C.-C. Liang, X. Xiao, X.-W. Gu, B. Chen, G. Qian, B. Li, Engineering Supramolecular Binding Sites in a Chemically Stable Metal−Organic Framework for Simultaneous High C_2H_2 Storage and Separation, Angew. Chem. Int. Ed. 61 (2022) e202211523.
[38] G.-D. Wang, R. Krishna, Y.-Z. Li, Y.-Y. Ma, L. Hou, Y.-Y. Wang, Z. Zhu, Rational Construction of Ultrahigh Thermal Stable MOF for Efficient Separation of MTO Products and Natural Gas, ACS Materials Lett. 5 (2023) 1091–1099, https://doi.org/10.1021/acsmaterialslett.3c00096.
[39] Y.-Z. Li, G.-D. Wang, R. Krishna, Q. Yin, D. Zhao, J. Qi, Y. Sui, L. Hou, A Separation MOF with O/N Active Sites in Nonpolar Pore for One-step C_2H_4 Purification from C_2H_6 or C_3H_6 Mixtures, Chem. Eng. J. 466 (2023) 143056, https://doi.org/10.1016/j.cej.2023.143056.
[40] H. Fang, B. Zheng, Z.H. Zhang, H.X. Li, D.X. Xue, J. Bai, Ligand-Conformer-Induced Formation of Zirconium-Organic Framework for Methane Storage and MTO Product Separation, Angew. Chem. Int. Ed. 60 (2021) 16521–16528, https://doi.org/10.1002/anie.202103525.
[41] Y.-L. Peng, T. Wang, C. Jin, P. Li, S. Suepaul, G. Beemer, Y. Chen, R. Krishna, P. Cheng, T. Pham, B. Space, M.J. Zaworotko, Z. Zhang, A robust heterometallic ultramicroporous MOF with ultrahigh selectivity for propyne/propylene separation, J. Mater. Chem. A 9 (2021) 2850–2856, https://doi.org/10.1039/d0ta08498k.
[42] L. Zhang, L.-N. Ma, G.-D. Wang, L. Hou, Z. Zhu, Y.-Y. Wang, A new honeycomb MOF for C_2H_4 purification and C_3H_6 enrichment by separating methanol to olefin products, J. Mater. Chem. A 11 (2023) 2343–2348, https://doi.org/10.1039/d2ta08977g.
[43] P. Zhang, X. Wen, L. Wang, Y. Zhong, Y. Su, Y. Zhang, J. Wang, J. Yang, Z. Zeng, S. Deng, Algae-derived N-doped porous carbons with ultrahigh specific surface area for highly selective separation of light hydrocarbons, Chem. Eng. J. 381 (2020) 122731, https://doi.org/10.1016/j.cej.2019.122731.
[44] L. Yang, X. Cui, Q. Yang, S. Qian, H. Wu, Z. Bao, Z. Zhang, Q. Ren, W. Zhou, B. Chen, H. Xing, A Single-Molecule Propyne Trap: Highly Efficient Removal of Propyne from Propylene with Anion-Pillared Ultramicroporous Materials, Adv. Mater. 30 (2018) 1705374, https://doi.org/10.1002/adma.201705374.
[45] G.-D. Wang, Y.-Z. Li, W.-J. Shi, L. Hou, Y.-Y. Wang, Z. Zhu, Active Sites Decorated Nonpolar Pore-Based MOF for One–step Acquisition of C_2H_4 and Recovery of C_3H_6, Angew. Chem. Int. Ed. 62 (2023) e202311654.
[46] G. Zhen, Y. Liu, Y. Zhou, Z. Ji, H. Li, S. Zou, W. Zhang, Y. Li, Y. Liu, C. Chen, M. Wu, Water-Stable Microporous Bipyrazole-Based Framework for Efficient Separation of MTO Products, ACS Appl. Mater. Interfaces. 16 (2024) 1179–1186, https://doi.org/10.1021/acsami.3c16968.
[47] G.D. Wang, Y.Z. Li, R. Krishna, W.Y. Zhang, L. Hou, Y.Y. Wang, Z. Zhu, Scalable Synthesis of Robust MOF for Challenging Ethylene Purification and Propylene Recovery with Record Productivity, Angew. Chem. Int. Ed. 63 (2024) e202319978.
[48] W. Fan, Y. Wang, Q. Zhang, A. Kirchon, Z. Xiao, L. Zhang, F. Dai, R. Wang, D. Sun, An Amino-Functionalized Metal-Organic Framework, Based on a Rare $Ba_{12}(COO)_{18}(NO_3)_2$ Cluster, for Efficient $C_3/C_2/C_1$ Separation and Preferential Catalytic Performance, Chem. Eur. J. 24 (2018) 2137–2143, https://doi.org/10.1002/chem.201704629.
[49] R. Krishna, Screening metal–organic frameworks for mixture separations in fixed-bed adsorbers using a combined selectivity/capacity metric, RSC Adv. 7 (2017) 35724–35737, https://doi.org/10.1039/c7ra07363a.
[50] R. Krishna, Methodologies for screening and selection of crystalline microporous materials in mixture separations, Sep. Purif. Technol. 194 (2018) 281–300, https://doi.org/10.1016/j.seppur.2017.11.056.
[51] X. Cui, K. Chen, H. Xing, Q. Yang, R. Krishna, Z. Bao, H. Wu, W. Zhou, X. Dong, Y. Han, B. Li, Q. Ren, M.J. Zaworotko, B. Chen, Pore chemistry and size control in hybrid porous materials for acetylene capture from ethylene, Science 353 (2016) 141–144, https://doi.org/10.1126/science.aaf2458.